Materials Science Forum Vols. 679-680 (2011) pp 145-152

doi:10.4028/www.scientific.net/MSF.679-680.145

A Comparative Study of the Morphologies of Etch Pits in Semi-insulating Silicon Carbide Single Crystals

Yan Peng[1, a], Xiangang Xua[1, b], Xiaobo Hu[1, c], Xiufang Chen[1, d] and Yuqiang Gao[1, e]

[1]State Key Laboratory of Crystal Materials, Shandong University, Jinan 250100, P.R.China

[a]penny4964@mail.sdu.edu.cn, [b]xxu@sdu.edu.cn, [c] xbh403@gmail.com, [d] cxiufang@mail.sdu.edu.cn , [e] gaoyuqiang2006@163.com

Keywords: semi-insulating SiC wafer, etching morphology, contactless resistivity mapping

Abstract: Contactless resistivity mapping, scanning electron microscope (SEM) and confocal laser microscope have been used to study the relationship of the resistivity and the etching behavior of the semi-insulating 6H-SiC wafer. Evidence is presented that the morphologies of the etch pits vary significantly with the impurity concentrations. The V impurity strongly affects the etch rates of edge, screw and mixed dislocations. For the dislocation containing the Burgers vector component of <0001>, its vertical etch rate is enhanced distinctly. In contrast, the horizontal etch rate becomes larger for the dislocation containing the Burgers vector component of $<11\bar{2}0>$. The shape of the etch pits reflects the Fermi level of the semi-insulating wafer and the net shallow impurity concentration.

Introduction

Much attention has been paid to the bulk SiC single crystals especially the semi-insulating SiC single crystals which can be used for the fabrication of high power/high temperature electronic devices [1]. Over the past several years, advancements in the PVT technology of SiC bulk growth have led to the commercial availability of 4 inch, high-quality, micropipe-free SiC substrate [2]. However, for common commercial SiC single crystals, there are still a large number of microscopic defects, such as dislocations and stacking faults. For example, the density of dislocation is in the order of 10^3-10^4cm^{-2} [2,3]. It has been noted that the dislocations degraded the performance and affected the long-term reliability of device [4].

To understand the microscopic defect formation mechanism and to further reduce the density of the microscopic defect are the main tasks of the recent research. Various techniques have been used to observe the dislocation in SiC crystal, such as X-ray diffraction, X-ray topography, transmission electron microscopy(TEM), wet etching (including conventional etching in aqueous solutions, electrochemical etching in electrolytes and defect-selective chemical etching in molten salts) and so on [5-10]. The simple, inexpensive and widely used method is defect-selective etching (DSE). Using optical microscopy, SEM and AFM, the different dislocations can be distinguished from the shapes and sizes of the etch pits. In the meantime, the densities and distributions of various dislocations can be obtained [10-14].

It has been found that the conduction behavior of the material and the Burgers vectors of dislocations were the crucial factors which affected the etching rates (vertical and horizontal etch rates), hence the etch pits' sizes and shapes. The larger the Burgers vectors, the larger the size of the etch pit [11]. It has been found that the isotropic etching was promoted in n-type SiC wafer, leading to round shape etch pits [12,15]. However, etch pits of the p-type material showed a more profound hexagonal shape [12,16]. Gao et al assumed these remarkable differences resulted from different dominated etching mechanisms. The electrochemical etching is dominant in n-type wafers, while the chemical etching was enhanced in p-type wafer [15]. At the same time, the etching rate of p-type material was lower by a factor of about 1.2 than that of the n-type SiC. It has been believed that the disparate activation energies of the etching process were, responsible for the different etching rates [12].

However, almost all studies mainly focused on the etch behavior of the n- and p- type wafer. In this paper, the etching behavior of the semi-insulating SiC was investigated. The morphologies of etch pits of different conductive type wafers were observed and compared. The samples of semi-insulating wafers were selected from the seed, middle and tail portion of a SiC boule. The observation results showed that morphologies of the etch pits were sensitive to the N and V impurity concentrations.

Experimental procedures

6H-SiC single crystals were grown by physical vapor transport (PVT) method. The growth temperature was kept in a range of 2400-2500K. In the growth procedure, V doping technique was employed to obtain the semi-insulating SiC single crystals. Boule I shows the n-type conductivity in the seed and semi-insulating in middle and high resistivity in the tail portion respectively. Different from boule I, boule II shows the n-type conductivity in the seed but exhibits semi-insulating behavior in both the middle and tail portions .

After crystal growth, the wafers were obtained from the cutting, lapping and polishing of SiC crystal boule. The samples named M1, T1 corresponded to the middle and tail portion of Boule I. For boule II, we named sample S2, M2 and T2 corresponding to the seed, middle and tail portion of the boule.respectively.

The etching was carried out in the molten KOH at 470°C for 10 min. The etch pits of dislocations was observed by optical microscopy, SEM and confocal laser microscopy. A contactless resistivity mapping (COREMA) system was used to measure the resistivities of the wafers.

A brief summary of the samples is listed in Table I. The FWHM are below 40 arcsec which demonstrate the good quality of the wafers. The etch pit densities are below $3.2 \times 10^4/cm^2$ in all the sample wafers.

Table I
Summary of the samples

Wafer ID	FWHM of X-ray rocking curve [arcsec]	EPD[/cm^2]	
		Screw dislocation	Edge dislocaton
S1	23	3.2×10^4	
M1	38	--	
T1	--	6.3×10^3	1.8×10^4
M2	--	1.4×10^4	
T2	30	7.4×10^3	1.5×10^4

Results and Discussions

The morphologies of etch pits of different conductive type wafer.

Fig.1 shows the contactless resistivity mapping the sample T1. The resistivity in the central region ($\rho>10^6\Omega$cm) is higher than that in the peripheral region ($\rho<10^5\Omega$cm). Since the concentrations of the shallow donors and acceptors gradually decrease during the whole growth process and stabilize at final stage corresponding to the tail portion of the boule [17], such resistivity distribution is caused by the nonuniformity of V incorporation.

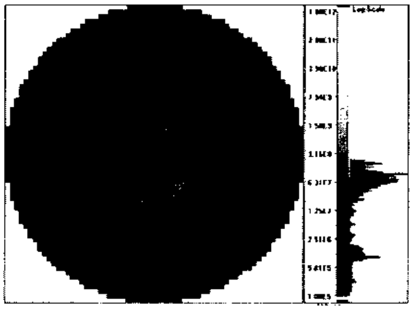

Fig.1. Resistivity mapping of the T1 measured by contactless resistivity measurement system. The variation of resistivity is shown by color alongside the map.

There are four kinds of dislocations in SiC single crystals, i.e. screw, edge, mixed and basal plane dislocation. All types of dislocations were observed by synchrotron X-ray topography. The X-ray topographic results show that the Burgers vector of the screw dislocation is 1c (b_s=<0001>=c); the edge dislocations are lying along <0001> with the Burgers vector of $1/3\langle 11\bar{2}0\rangle$ ($b_e=1/3\langle 11\bar{2}0\rangle$=a,); for mixed dislocation, the Burgers vector contains the components of <0001> and $1/3\langle 11\bar{2}0\rangle$ ($b_m=\sqrt{a^2+c^2}$); and the basal plane dislocations are the pure screw dislocation lying along $\langle 11\bar{2}0\rangle$ direction with the Burgers vector of $1/3\langle 11\bar{2}0\rangle$ ($b_b=1/3\langle 11\bar{2}0\rangle$=a) [7].The sequence in sizes of the Burgers vector of the threading dislocations is as follows: MD>SD>ED. The disparity of the Burgers vectors of the various dislocations result in the different etching rates. The larger the Burgers vectors, the larger the size of the etch pit [11]. It helps us to distinguish the types of the dislocations. Fig.2 shows the SEM images of etch pits in the peripheral region ($\rho<10^5\Omega$cm). The largest etch pit which is a distinct hexagon with a large black core forming from the outcrop of screw dislocation (labeled by SD). The size of the etch pit is 17 μm. The smallest one whose diameter is 11 μm and depth is shallower than SD corresponds to an edge dislocation (labeled by ED). The middle-size one with a diameter of 15 μm has a small black core and results from a mixed dislocation (labeled by MD). The etch pits of the three kinds of dislocations are perfect hexagons with the six-fold symmetry and have steps on the sides of the etch pits.

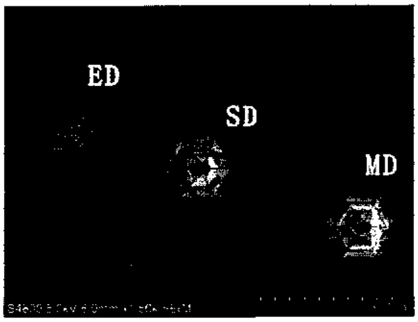

Fig.2 The etch pits in the peripheral region ($\rho < 10^5 \Omega cm$) show different morphologies. They originate from different dislocations, such as screw dislocation(SD),edge dislocation(TD) and mixed dislocation(MD).

The morphologies of the etch pits in the center part of the T1 ($\rho > 10^6 \Omega cm$) exhibit remarkably different characteristics from those in periphery region. The SEM images of the etch pits in central region with a 30° tilt of sample are shown in Figure 3 (a), (b), (c) and (d) corresponding to screw, mixed, edge and basal plane dislocation, respectively. The size of the etch pits of the edge dislocation (fig.3(c)) is two times larger than that in Fig.2. For other dislocations, the size of etch pits are almost the same. However, the sectional morphologies of etch pits change with different Burgers vectors of dislocations. The etch pits of screw dislocation and mixed dislocation have the hollow cores extending along <0001> direction. The inclination angle of the side walls is much larger. To observe clearly the bottom of the etch pit, the 3D image of the back view of the etch pits are obtained by the confocal laser microscopy. The hollow cores of screw dislocation are an empty tube with a flat bottom. The etch pit of edge dislocation assumes a triangular shape with a sharp bottom.

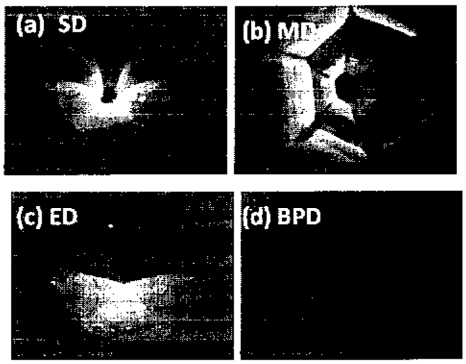

Fig.3. The SEM images of etch pits in the center region of T1 ($\rho > 10^7 \Omega cm$). These etch pits originate from screw dislocation (SD), mixed dislocation (MD), edge dislocation (ED) and basal plane dislocation (BPD) respectively. The images were taken with the 30° tilt of sample.

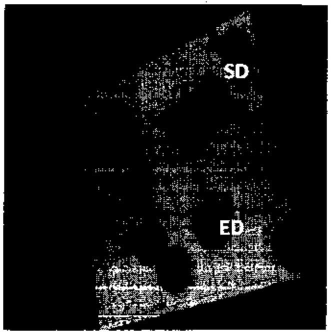

Fig.4. The 3D image of the back view of the etch pits observed by the confocal laser microscopy ($\rho > 10^7 \Omega$cm). The etch pit of the screw dislocation (SD) has a flat bottom with hollow tube. The etch pits with a sharp bottom corresponds to an edge dislocation(ED).

All above results implied that the concentration of V impurity affects the vertical and horizontal etch rates, hence, the etch pits sizes and shapes of the various dislocations. For a dislocation containing the Burgers vector component of $<0001>$, the vertical etch rate is enhanced distinctly. While the horizontal etch rate becomes larger for a dislocation containing the Burgers vector component of $<11\bar{2}0>$.

The morphologies of etch pits of semi-insulating wafer.

The shapes of etch pits in semi-insulating SiC are different from those in n-type SiC. The resistivity and the morphologies of the etch pits of M2 and T2 are shown in Fig.5. The resistivity of M2 is higher than $1\times10^9 \Omega$cm and the radial resistivity variation is within one order of magnitude. The SEM image of the etch pits of M2 (Fig. 5(b)) shows that all of the etch pits are round and it is hard to distinguish the various kinds of the dislocations. However, for the sample T2, the shape of the etch pits becomes perfect hexagons and the resistivity is above $1\times10^8 \Omega$cm as shown in fig. 5(c).

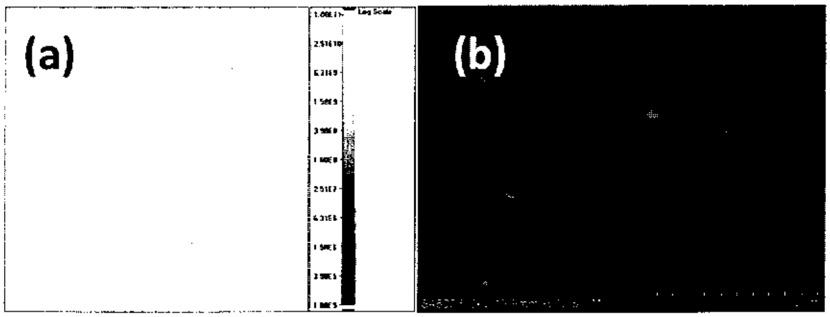

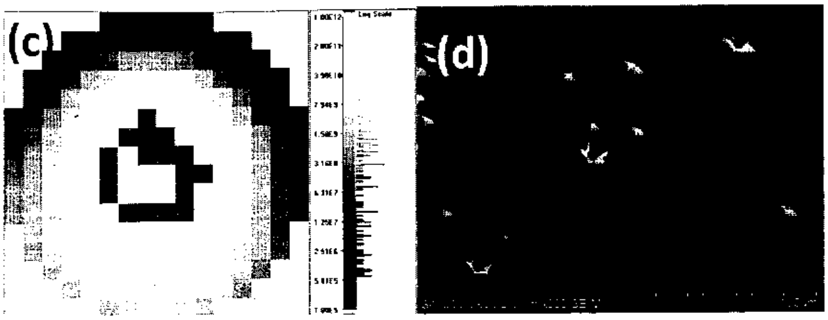

Fig.5 Dependence of the resistivity and the shape of etch pits: (a) Contactless resistivity map of the sample M2; (b) The SEM image of M2 with a 25° tilt of sample; (c) Contactless resistivity map of the sample T2;(d)The SEM image of T2 with a 25° tilt of sample.

In order to reveal the relationship between the shape of the etch pits and the conductivity type, we measured resistivities and observed the morphologies of etch pits at ten different positions.

Table Π The relationship between the shape of the etch pits and the conductivity type

Wafer ID	Sample position	Resistiviy[Ωcm]	The morphologies of etch pits
S1	Center	$<1\times10^5$	Round
	Edge	$<1\times10^5$	Round
M1	Center	2.04×10^{11}	Round
	Edge	5.97×10^9	Round
T1	Center	3.92×10^6	Hexagons
	Edge	$<1\times10^5$	Hexagons
M2	Center	1.59×10^{10}	Round
	Edge	2.41×10^{10}	Round
T2	Center	1.64×10^{11}	Hexagons
	Edge	6.55×10^8	Hexagons

The above results clearly suggest that: (i) the morphologies of the etch pits are not directly related with the resistivity of the wafer, (ii) in the seed and middle part of the boules, the etching is isotropic, and (iii) only in the tail part, the etch pits become perfect hexagons. These etching behaviors indicate that the electrochemical reaction are involved although the wafers are semi-insulating.

The electrochemical reaction in the etch process is discussed by YingGao et.al[15,18]. It was shown that two parallel reactions exist in the molten KOH etching of SiC: one is a chemical reaction, and the other one is an electrochemical reaction. For p-type SiC, the the energy band bends downward at the SiC/solution interface and a depletion layer is formed in the surface. Without the free carrier in this layer, the chemical reaction takes place and the etching is preferential. However, for n-type SiC, the electrochemical reaction dominates due to an inversion layer with high density of the holes caused by the significant upward energy band bending. The etching with electrochemical reaction is isotropic.

For the semi-insulating wafers obtained by the V doped techniques, there are two possible deep levels. One is V^{3+}/V^{4+} acceptor level about 0.8eV below the conduction band. As the fermi level is located in the upper half of the band gap, electrons excited from V^{3+} to the conduction band lead to the small remaining n-type conductivity. Another deep level is V^{4+}/V^{5+} donor level about 1.5 eV which is approximate the middle of the band-gap. In other words, the Fermi level of the semi-insulating wafer is determined by the net of N_A and N_D [19-21].We believe the nitrogen concentration decreases exponentially along the growth direction and boron content is stable during the growth process[17]. If the N_A-$N_D > 0$, the Fermi level of the semi-insulating wafers changes from 0.8eV to 1.5eV and the etching behaviors become anisotropic. All the results implied that the shape of the etch pits reflects the Fermi level of the semi-insulating wafer and the net shallow impurity concentration.

Summary

In summary, the etching behavior of the semi-insulating 6H-SiC wafer was observed and analyzed .The results are presented that the concentration of V impurity changes the the vertical and horizontal etch rates of various dislocation, hence the shape and the size of the etch pits. The resistivity of the wafer does not play a significant role in affecting the morphologies of the etch pits. The shape of the etch pits in semi-insulating wafer reflects the Fermi level.

Acknowledgements

This work was supported by the National Natural Science Foundation of China under grant No. 50721002 and 50802053, National Basic Research Program of China under grant No. 2009CB930503 and No.2011CB301904.

Reference

[1] S.Sriram, R.C.Clarke, A.A.Burk,H.M.Hobgood, T.J.Smith, C.D.Brandt and R.H.Hopkins: IEEE Elecron Dev.Lett. Vol. 15(1994), p.458

[2] E. Berkman, R. T. Leonard, M. J. Paisley, Y. Khlebnikov, M. J. O'Loughlin,A. A. Burk, A. R. Powell, D. P. Malta, E. Deyneka, M. F. Brady, I. Khlebnikov,V. F. Tsvetkov, H. McD. Hobgood, J. Sumakeris, C. Basceri, V. Balakrishna,C. H. Carter, Jr. and C. Balkas: Materials Science Forum Vols. 615-617 (2009), p.3

[3] H.-J. Rost, M. Schmidbauer, D. Siche and R. Fornari: Journal of Crystal Growth Vol.290 (2006), p.137

[4] H. Lendenmann, F. Dahlquist, J.P. Bergman, H. Bleichner and C.Hallin: Materials Science Forum Vols. 389 - 391 (2002), p.1259

[5] Shizhong Wang, Jibao He: Materials Science and Engineering Vol.B83 (2001), p.8

[6] R.Tanuma, T.Tamori, Y.Yonezawa, H.Yamaguchi, H.Matsuhata,K.Fukuda and K.Aral: Materials Science Forum Vols.615-617(2009), p.251

[7] Daisuke Nakamura, Satoshi Yamaguchi, Itaru Gunjishima,Yoshiharu Hirose and Tsunenobu Kimoto: Journal of Crystal Growth Vol.304 (2007), p.57

[8] Michael Dudley,Yi Chen, XianRong Huang and Ronghui Ma: Materials Science Forum Vols.600-603(2009), p.261

[9] T.Nishiguchi, T.Furusho, T.Isshiki,K.Nishio,H.Shiomi and S.Nishino: Materials Science Forum Vols.600-603(2009),p.329

[10] D. Zhuang, J.H. Edgar:Materials Science and Engineering Vol R 48 (2005),p. 1

[11] J.L. Weyher: Superlattices and Microstructures 40 (2006) 279–288

[12] S.A. Sakwe, R. Müller, P.J. Wellmann: Journal of Crystal Gprowth Vol.289 (2006) ,p.520

[13] D. Siche, D. Klimm, T. H. olzel, A. Wohlfart: Journal of Crystal Growth Vol.270 (2004) ,p.1

[14] Erwin Schmitt, Thomas Straubinger, Michael Rasp,Arnd-Dietrich Weber: Superlattices and Microstructures Vol.40 (2006), p. 320–327

[15] Ying Gao, Zehong Zhang,Rober Bondokov,Stanislav Soloview and Tangali Sudarshan: Mat.Res.Soc.Symp.Proc. Vol.815(2004),p.J5.20.1

[16] Sakwe Aloysius Sakwe, Mathias Stockmeier, Philip Hens, Ralf Müller, Desirée Queren,Ulrike Kunecke, Katja Konias, Rainer Hock, Andreas Magerl, Michel Pons, Albrecht Winnacker,and Peter Wellmann: phys. stat. sol.(b) Vol.245(2008),p.1239

[17] Q. Li, A. Y. Polyakov, M. Skowronski,E. K. Sanchez , M. J. Loboda,M. A. Fanton, T. Bogart, and R. D. Gamble:Journal of Applied Physics Vol .97 (2005),p.113705

[18] J.S.Shor, R.M.Osgood, and A.D.Kurtz: Applied Physics Letter Vol.60 (1992), p.1001

[19] M. Bickermann, R. Weing.artner,and A. Winnacker: Journal of Crystal Growth Vol.254 (2003),p.390

[20] J.R.Jenny, M.Skowronski, W.C.Mitchel, H.M.Hobgood, R.C.Glass, G.Augustine, and R.H.Hop: Journal of Applied Physics Vol.78 (1995), p.3839

[21] H. McD. Hobgood, R. C. Glass, G. Augustine, R. H. Hopkins, J. Jenny, M. Skowronsk ,W. C. Mitchel ,and M. Roth: Applied. Physic s. Letter. Vol.66(1995), p.1364